Journal of Sound and Vibration 483 (2020) 115496

Contents lists available at ScienceDirect

Journal of Sound and Vibration

journal homepage: www.elsevier.com/locate/jsvi

Considerations about the applicability of the Reynolds equation for analyzing high-speed near field levitation phenomena

Noël Brunetière [a], Michał Wodtke [b, *]

[a] Institute Pprime, CNRS Université de Poitiers, Ensma, UPR 3346, Dépt Génie Mécanique et Systèmes Complexes SP2MI, 11 Bd Marie et Pierre Curie, 86360, Chasseneuil Du Poitou, France
[b] Gdansk University of Technology, Faculty of Mechanical Engineering, Narutowicza 11/12, 80-233, Gdansk, Poland

ARTICLE INFO

Article history:
Received 20 October 2019
Received in revised form 16 April 2020
Accepted 1 June 2020
Available online 7 June 2020
Handling Editor: L. Huang

Keywords:
Near field levitation
Reynolds equation
CFD
High frequencies

ABSTRACT

This paper presents the results of investigations into the applicability of the Reynolds equation for analyzing near field levitation (NFL) phenomena. Two separate approaches were developed, experimentally verified, and applied to meet the research objective. One was based on the Reynolds equation and the other was based on general conservation equations for fluid flow solved using computational fluid dynamic (CFD). Comparing the calculation results revealed that, for certain operating conditions, differences in the predicted system parameters appear. It was proven that both the Reynolds and Helmholtz numbers define border operating conditions for the applicability of the Reynolds equation to analyze NFL problems.

1. Introduction

The possibility to levitate objects offers an interesting alternative to eliminate friction and adhesive forces in microsystems and allow accurate and controlled displacements of micro-objects [1,2]. Among all the possible technical solutions, Vandaele et al. [1] indicated that acoustic levitation is the most interesting solution because it is more versatile than other methods. The levitation is provided by a vibrating plate that modifies the air pressure distribution between the plate and the object, leading to a net force able to balance the weight of the object. Depending on the ratio of the air gap, h, to the acoustic wavelength, λ, two levitation modes can be identified [1]. If h is higher than λ, this is standing wave levitation; otherwise, it is near field levitation (NFL) or squeeze film levitation [2].

NFL, which provides much higher force [1], is the topic of this paper. One of the first experimental studies of squeeze film levitation was performed by Salbu in 1964 [3]. A piston-like motion of the bottom plate was imposed by an electromagnetic actuator, allowing Salbu to measure the net force value as a function of the average distance between the plates. The piston-like motion, which can be easily measured and theoretically modeled, was adopted in several later studies where the electromagnetic actuator was replaced by a more efficient piezoelectric actuator [4–8]. This solution can provide high levels of levitation force, estimated as up to 70 kNm^{-2} by Ueha et al. [6]. Even if, in many studies, the system was operated at its natural oscillation frequency (generally corresponding to several tenths of 1 kHz) to reduce the energy needed for actuating

* Corresponding author.
E-mail addresses: noel.brunetiere@univ-poitiers.fr, michal.wodtke@pg.edu.pl (N. Brunetière), mwodtke@pg.edu.pl (M. Wodtke).

https://doi.org/10.1016/j.jsv.2020.115496

Nomenclature

a	ms^{-1} speed of sound
e	m oscillation amplitude
f	Hz oscillation frequency
F_{aero}	N aerodynamic force
g	ms^{-2} gravitational acceleration
h	m average levitation height
H	- Helmholtz number
Kn	- Knudsen number
m	kg mass of the levitating object
M	kg mol^{-1} molar mass
p	Pa pressure
p_a	Pa atmospheric pressure
r, β, z	m cylindrical coordinates
R	J mol^{-1} K^{-1} gas constant
R_d, L	m radius (width) of the levitating object
Re	- Reynolds number
t	s time
T	K temperature
$\mathbf{U}$	ms^{-1} velocity vector
λ	m acoustic wavelength
λg	m mean free path of the gas
μ	Pa s dynamic air viscosity
ρ	kg m^{-3} density of the air
σ	- squeeze number
τ	Nm^{-2} stress tensor
ω	rad s^{-1} angular frequency (pulsation of the vibration)

the bottom plate, a very stiff and massive plate is usually needed to ensure perfect motion of the top surface. To reduce the thickness of the bottom plate and allow lateral size increases, it was necessary to operate the system at its structural flexural mode. In this case, the bottom plate motion is more complex and controlled by structural dynamic behavior. This solution was adopted in many papers [6,9–11]. This approach has been extended to create journal bearings [12–17] or methods to move the levitated objects [18–22]. In addition, the vibrating motion of the bottom plate can lead to the flexural vibration of the top plate, which makes the problem more complex [23].

The airflow between the vibrating plate and the levitated object is governed by the general Navier-Stokes set of equations. Depending on the configuration, some physical contributions vanish, and the equations can be simplified. When the levitation distance, h, is small compared to the characteristic width of the object, L, viscous effects are dominant and inertia effects in the fluid are negligible. It is thus possible to use the Reynolds equation to describe the flow in the air gap [24]. This approach has been successfully used by many authors [3,8,25–29]. When the configuration is axisymmetrical and the air gap is a sine function of time, the Reynolds equation has an analytical solution involving Kelvin functions, as demonstrated by Crandall [25]. Crandall also showed that two regimes exist, depending on the value of what is currently named the squeeze number: $\sigma = 12\ \mu\ \omega\ R_d^2/(p_a\ h^2)$ where μ is the viscosity of air, ω is the vibration pulsation, R_d is the outer radius of the system, h is the average gap, and p_a is the atmospheric pressure. At low squeeze numbers, the flow is mainly viscous, leading to a high damping coefficient for the film and low stiffness. However, at high squeeze numbers, the compressibility effect becomes dominant, damping is low, and the stiffness is maximal [25,27]. In this last regime, the fluid behaves as an enclosed mass of air that is compressed between the plates without any radial flow. The gas film can be described by Boyle's law [3,29].

If it is assumed that the oscillating motion is fast enough so that no viscous fluid motion is observed, the Navier-Stokes equations can be reduced to the Euler set of equations. The pressure distribution can thus be obtained from acoustic theory [2,5,6]. If the lateral size of the domain is large compared to the wavelength, λ, of acoustic waves, an analytical solution of the pressure is obtained. It can be further simplified in the case of near field acoustic levitation ($h >> \lambda$) ([2,5,6]). Using this simplified solution, it can be shown that the average levitation height, h, is proportional to the vibration amplitude, e, of the bottom plate and inversely proportional to the square root of the mass, m, of the levitated object. The same solution is obtained with the Reynolds equation at high σ value or with Boyle's law [8].

Based on this last finding, it can be postulated that the Reynolds solution, which has the advantage of being solved at low computation cost, can be used to solve all near field problems. However, depending on the operating conditions, many authors found that additional effects not considered in the Reynolds equation must be accounted for. Andrews et al. [27]

performed some tests at low ambient pressure (80 Torr) and showed that the rarefaction effect, inducing slip of the air on the plates, must be considered. Indeed, in this case, the mean free path of the gas, λg, is increased, leading to high values of the Knudsen number, $Kn = \lambda g/h$. Based on the Knudsen definition, rarefaction effects can also be observed at low film thickness values, h [30]. Mohite et al. [30] also showed that fluid inertia can affect the behavior of the squeeze film when the magnitude of the Reynolds number, $Re = \rho\omega h^2/\mu$, is higher than 1. For small Re values, Stolarski and Chai [31] verified that the Reynolds equation is relevant. Li et al. [32] also included the effect of convective inertia in a modified Reynolds equation. In addition, they considered the pressure drop occurring during fluid suction in the contact due to the sudden section reduction at the inlet. They showed that this effect becomes significant when the squeeze number increased. However, Minikes and Bucher [33] showed that edge effects, manifested as a pressure difference at the inlet, can be observed at low squeeze numbers due to flow interaction with the oscillating plate when the plate is bigger than the levitated object. Finally, in the case when one of the plates rotates, centrifugal inertia effects can be experienced [29]. This last point is beyond the scope of this work. These additional effects can make the Reynolds equation ineffective for solving the levitation problem, particularly when high oscillating frequencies are considered. As previously discussed, high operating frequencies are encountered in many applications where the system is used at its natural frequency. However, the limit of using Reynolds has not been clearly identified for this type of squeeze problem.

In this work, simulations were carried out with Navier-Stokes equations and the Reynolds equation. The results were compared to find the limit of validity for the Reynolds equation. Some deviations are observed at high oscillating frequencies and are related to acoustic wave propagation in the contact. It was possible to define a dimensionless number equivalent to the Helmholtz number to identify the limit of validity for the Reynolds equation.

2. Goal and scope of the research

The Reynolds equation was derived from general fluid dynamics conservation equations using a number of simplifying assumptions, one of them is neglecting fluid inertia. The goal of this work is to determine the range in which the assumptions of the Reynolds equation are acceptable for analyzing NFL problems. For this purpose, calculations of the piston-like motion system were carried out using two separate computational models that differ in their description of airflow in the air gap: a) a model using general fluid dynamics conservation equations, b) a model using the Reynolds equation. The developed models considered both time-varying flow in the air gap and the movement of the levitated mass caused by aerodynamic force. Investigations were carried out for object geometry and oscillation parameters accessible at the test stand. Selected results of the experimental tests were also used to verify the correctness of developed models.

The calculations were carried out using both theoretical models for the same operating conditions and oscillation frequencies of the plate, assumed in a wide range. A comparison of the calculated levitation parameters showed differences between the results and determined the validity range of the results obtained from solving the Reynolds equation for analyzing an NFL system. The research was carried out assuming that the oscillating mass and the oscillating plate remain rigid during operation. That simplification may influence the whole system behavior if relatively elastic elements were applied (thin and/or with a large diameter). However, despite of this assumption, conclusions about applicability of different approaches for investigations of the air flow in the gap, which is the goal of this paper, remain valid.

3. Problem description

The principle of obtaining load capacity in an aerodynamic gas film, as a result of forced oscillations using a piston-like motion system, is illustrated schematically in Fig. 1. An oscillating plate, as a result of actuator operation, is nominally introduced into uniaxial oscillations. Above the plate, the levitating mass (disk-shaped) is placed. Between those elements, due to forced sinusoidal oscillations, an aerodynamic lubricating film is formed (on the principle of squeeze film effect). During system operation, pressure in the film exerts force on the levitated mass and causes its lift. As a result, a levitated mass is also introduced into oscillations, the amplitude of which depends on the frequency of the oscillating plate.

4. Methodology

Taking into account the operating principle of NFL, the aerodynamic film parameters (e.g. pressure field or film thickness) should be analyzed in the time domain. This applies both to the flow in the air gap and the displacement of the surfaces limiting it: the oscillating plate and levitated mass. In the described problem, oscillating plate displacement is imposed and known while the mass elevation distance and its oscillations are the result of forces acting on the object and could be calculated using the fundamental dynamics law of motion.

It was assumed that airflow was isothermal, laminar, without external forces acting on the fluid and air satisfies the ideal gas assumptions. Within the scope of this work, two different approaches for describing airflow were implemented: a) The computational fluid dynamics model (CFD model) based on the solution of the set of general conservation equations of the fluid flow, which for a Newtonian fluid, reduces to the Navier-Stokes set of equations, b) Reynolds model based on the solution of the Reynolds equation.

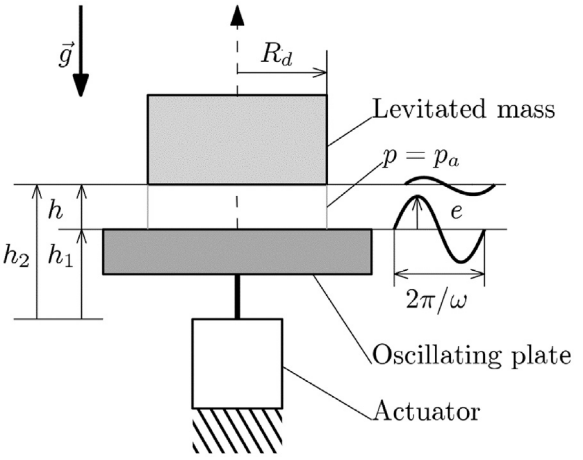

Fig. 1. Configuration of the problem.

4.1. CFD model

The model was developed using the CFX package [34], which uses the finite volume method for discretizing and solving 3D conservation equations for transient flow of compressible fluids:

$$\text{the continuity equation: } \frac{\partial \rho}{\partial t} + \nabla \cdot (\rho \mathbf{U}) = 0 \tag{1}$$

$$\text{the momentum equations: } \frac{\partial (\rho \mathbf{U})}{\partial t} + \nabla \cdot (\rho \mathbf{U} \otimes \mathbf{U}) = -\nabla p + \nabla \cdot \boldsymbol{\tau} \tag{2}$$

which, together with the ideal gas equation of state:

$$\rho = \frac{Mp}{RT} \tag{3}$$

allows obtaining a solution to the air gap flow problem. The following symbols are used in equation (1) – (3): ρ - air density, t - time, $\mathbf{U}$ - velocity vector, p - pressure, $\boldsymbol{\tau}$ - stress tensor, M - air molar mass (28.96×10^{-3} kg mol^{-1}), T - temperature, R - gas constant (8.314 J mol^{-1} K^{-1}). Since air is Newtonian fluid, stress tensor $\boldsymbol{\tau}$ (in equation (2)) is proportional to velocity gradients $\nabla \mathbf{U}$ and dynamic viscosity μ, according to equation (4):

$$\boldsymbol{\tau} = \mu \left(\nabla \mathbf{U} + (\nabla \mathbf{U})^{\mathrm{T}} - \frac{2}{3} \delta \nabla \cdot \mathbf{U} \right) \tag{4}$$

where: δ is the Identity matrix. Mathematical operators in equations (1)–(4) are: '$\nabla\cdot$' divergence, '$\mathbf{U} \otimes \mathbf{U}$' is the dyadic operator of velocity vectors $\mathbf{U}$ and ∇ is gradient.

Taking advantage of axial symmetry, the developed discrete model was simplified so that it represents only a part of the air gap with symmetry boundary conditions at the side walls (Fig. 2). At the outer wall of the model, an opening boundary condition was defined with the value of total pressure equal to ambient pressure. At the bottom and top walls, a 'no-slip' boundary condition was imposed. The bottom wall represents the surface of the oscillating plate and its displacement was imposed on the vertical axis (z in Fig. 2) using 'mesh motion' capability, according to Equation (5):

$$h1 = -e \cdot \sin(2 \cdot \pi \cdot f \cdot t) \tag{5}$$

where: $h1$ is the imposed position of the oscillation plate in vertical direction as a function of time t, e is the oscillation amplitude, f is the oscillation frequency.

The top wall of the CFD model represents the surface of the levitated mass. To include the interaction between the levitated object and air gap pressure, the Rigid Body solver was employed. Rigid Body is a simplified form of fluid-structure interaction (FSI) available in CFD software allowing to analyze the body response to flow forces under the assumption that the body does not change shape under fluid load [34,35].

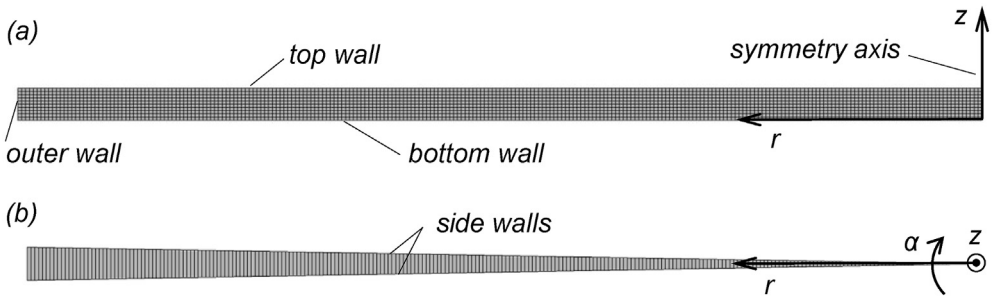

Fig. 2. Schematic view of the CFD mesh, (a) side view; (b) top view.

It was assumed, considering the symmetry of the analyzed problem, that movement of the levitated mass was only possible in the vertical direction (1 DOF option). Consequently, the top wall movement was obtained with the Rigid Body solver using the solution of the dynamic equation of motion for one direction (using the Newmark integration scheme):

$$m\ddot{z} = F_{\text{aero}} + mg \tag{6}$$

where m is the mass of the levitated object, kg; $\ddot{z}$ is the object's acceleration, ms^{-2}; F_{aero} is the force in the air gap due to the squeeze effect, N; and g is gravitational acceleration, ms^{-2}.

Analyses were carried out using a mesh divided into 500 finite volumes in the air gap radial direction, 20 in the film thickness direction and one in the circumferential direction. Mesh parameters were determined using the results of a mesh independence study. Angular size of the grid was assumed $\alpha_g = 1^\circ$, to get its adequate quality. Calculations were started with the assumed initial air gap thickness (usually 5 μm). During calculations, the thickness of the air gap changed as a result of interaction between structural and aerodynamic loads. Calculations were stopped after obtaining a stable and repeatable oscillating movement of the upper surface (levitation mass). Each oscillation period was divided into 400 time steps. To achieve stable elevation of the levitated object and repeatable oscillations, one calculation task required, depending on the case, from several to hundreds of analyzed periods of enforced oscillation.

4.2. Reynolds model

The model using the solution of the Reynolds equation to describe flow in the air gap of an NFL problem, which was applied in this study, was presented in detail in work [8]. The equations were solved with the use of an own devised code written in Fortran 2003 and based on the Finite Volume Method. As discussed in the introduction, the Reynolds equation is a simplification of the Navier-Stokes equations, due to the thin film configuration where only a part of the viscous contributions are preserved [24]. Therefore, the inertia terms are neglected and the pressure is constant in the through film direction. The fluid velocity profiles are thus parabolic and proportional to the radial pressure gradient.

The Reynolds model, similar to the CFD model, used the axial symmetry of the analyzed system (for simplifying calculations) and the same set of boundary conditions and assumptions for air behavior in the gap (ideal gas). In addition, movement of the oscillation plate was imposed using Equation (5) and the levitated mass had one degree of freedom, with position calculated using the dynamic law of motion with Equation (6), as for the CFD model.

4.3. Input data

The geometrical and physical parameters of the system, as well as operating conditions used in analyses, are shown in Table 1. The air dynamic viscosity was assumed to be $\mu = 1.831 \times 10^{-5}$ Pa s, gravitational acceleration was $g = 9.81\ \text{ms}^{-2}$ and temperature was $T = 300$ K.

Table 1
Problem input data.

parameter	value
mass, m	19.28×10^{-3} kg
mass radius, R_d	15 mm
oscillation amplitude, e	1 μm
oscillation frequency, f	2–60 kHz

5. Results

5.1. Experimental validation

The correctness of the developed theoretical models was evaluated using the results of experimental measurements obtained using a test stand in the piston-like-motion NFL problem configuration. Details regarding the construction of the test stand were presented in Ref. [8]. Due to the limitations of the test stand, it was only possible to carry out measurements for oscillation frequencies up to 4 kHz. Test parameters were the same as shown in Table 1. Each test was repeated three times. The maximum difference in the average mass distance between the different tests is 0.2 μm, which indicates an excellent reproducibility of the experiments.

Fig. 3 shows a comparison of the measured and calculated values of average levitated mass distance (a) and mass RMS (Root Mean Square) displacement (b). Similar average levitated mass distances were calculated using both models (the maximum relative difference was not larger than 3.5%). Measured values differ from calculated ones, especially for low frequencies; however, for frequencies over 3 kHz, good agreement was observed. Slightly better agreement observed for the Reynolds approach results is rather accidental and is probably caused by uncertainty of the experimental data. Surfaces flatness errors or deviations from assumed oscillating plate motions are possible examples of measurement inaccuracies sources.

Two initial points from the experimental research show measured film thickness under conditions of non-fully developed squeeze film lubrication. Direct contact between both surfaces took place for lowest tested frequencies. Such situation was not possible to consider with the use of developed methodology for investigations of NFL system operation.

In the case of the RMS value of levitated mass displacement, which is a measure of similarity of calculated and experimentally observed oscillations of the levitated object, very good agreement was noticed for the whole analyzed range of frequencies.

The comparison of the calculated and measured parameters of NFL proved the correctness of the results obtained from theoretical models and the differences could be explained mainly by the difficulties and uncertainties in experimental tests, such as flatness defects in the surfaces, non-perfect sinusoidal motion, and height measurement uncertainty.

Experimental validation of the theoretical results for high frequencies was not possible with the use of available equipment. Good agreement for low frequencies confirmed, that both models work well, and predicted parameters of NFL system were very close to the measured data. However, when one tries to expand that statement also for high frequencies, it can be assumed that simplifications introduced to the Reynolds approach (e.g. assumption of parabolic velocity profile across gap or no inertia effects) can lead to not adequate results, because flow inertia has presumably strong influence on operating parameters of the system in such conditions.

5.2. Parametric study

Parametric studies were carried out for the frequency range of the oscillating plate, from 2 to 60 kHz. The calculated average mass distance is compared in Fig. 4.

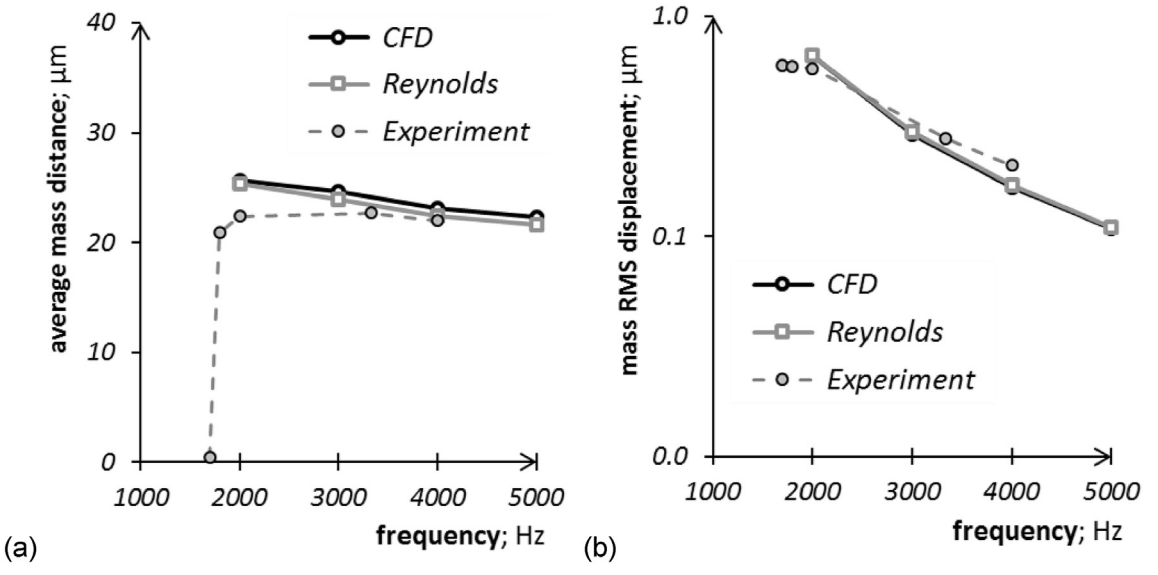

Fig. 3. Comparison of the results of calculations and measurements; (a) average mass distance, μm; (b) mass RMS displacement, μm.

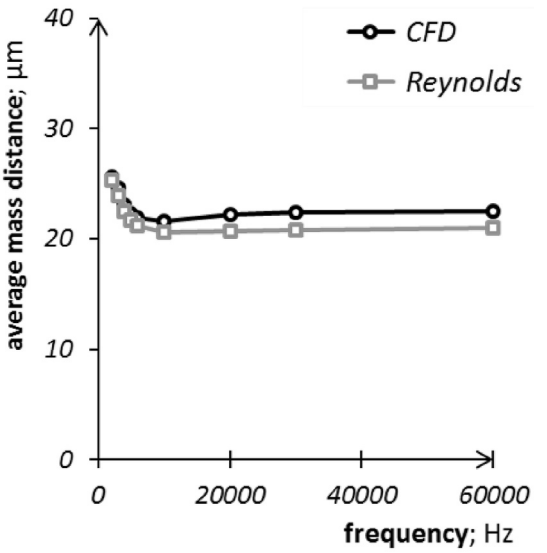

Fig. 4. Average mass distance, µm, as a function of oscillation frequency, comparison between CFD and Reynolds model results.

The highest mass levitation height was obtained for the lowest analyzed frequency. With increased oscillation frequency up to 10 kHz, mass lift distance decreased. At higher excitation frequencies (>10 kHz), the lifting height did not depend strongly on the oscillation frequency. It is worth noting that results obtained from both theoretical models showed the same trend of changes, whereas average mass lift distances calculated using CFD were slightly higher than those obtained from the Reynolds model. However, differences in results for frequencies <6 kHz were relatively low (about 3%). For higher oscillation frequencies, differences between the results of CFD and Reynolds models were slightly higher (up to 8%).

In Fig. 5, the calculated maximum air flow rate at the gap border (inlet/outlet) (a) and maximum air gap pressure (b) are compared. Similar to the average mass distance, the trend of changes for air flow rate as a function of frequency, predicted using both models, was the same (Fig. 5a). Except for the initial frequency range ($f < 4$ kHz), the flow rate increased with increasing oscillation frequency; while for frequencies above 20 kHz, the calculated flow rate using the Reynolds model was higher than for CFD.

The trends of maximum pressure changes in the film (Fig. 5b) calculated by the CFD and Reynolds models look slightly different. In the initial frequency range for both models (<20 kHz), the maximum pressure in the film decreased with increasing frequency. For higher frequencies, this trend is also visible in the results obtained from the Reynolds model;

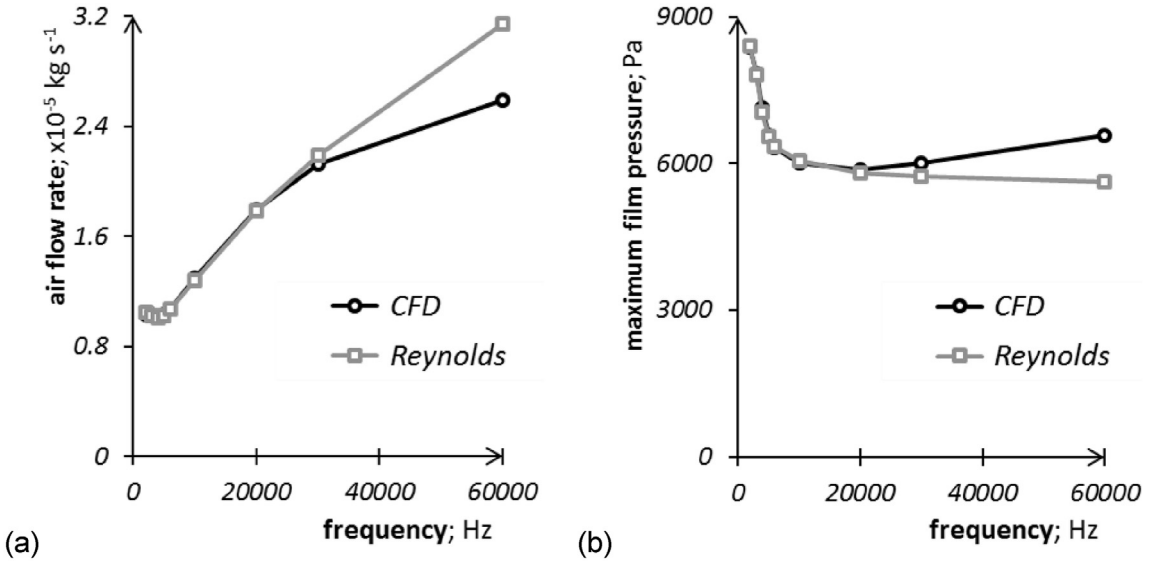

Fig. 5. Air flow rate, x10^{-5} kg s^{-1}; (a) and maximum film pressure, Pa (b) as a function of oscillation frequency, comparison between CFD and Reynolds model results.

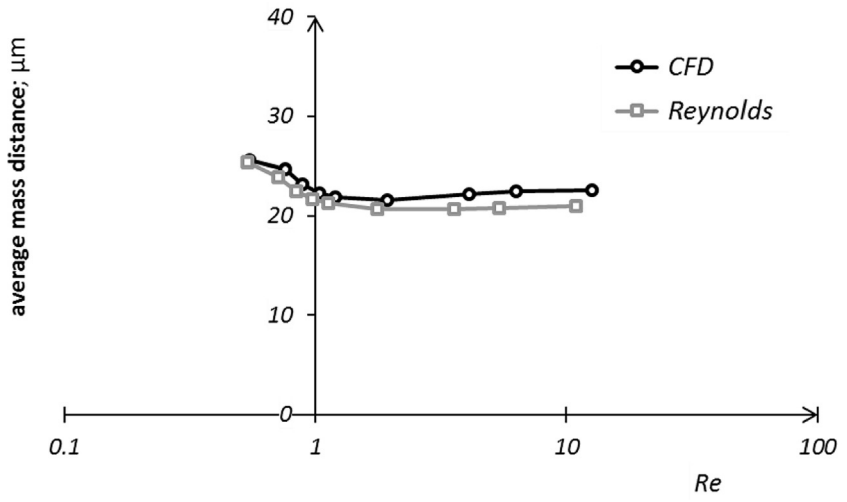

Fig. 6. Average mass distance, µm, as a function of Reynolds number, comparison between CFD and Reynolds model results.

however, the calculated change in the maximum pressure value was relatively small. The opposite trend was noticed for results obtained from the CFD model, which for frequencies >20 kHz, the calculated maximum pressure in the air film increased with increases in the oscillation frequency.

In the case of analyzed quantities at frequencies up to 20 kHz, both models predicted nearly identical parameter values (Fig. 5). For higher frequencies (>20 kHz), a comparison of the results obtained from the CFD and Reynolds models shows visible differences, which increase with increasing oscillation plate frequency.

6. Discussion

The derivation of the Reynolds equation assumes that the inertia effects in the flow are negligible. Consequently, one of the main reasons for the deviation between the Reynolds and CFD solutions is the appearance of a significant inertia effect. Based on the work of Mohite et al. [30], the Reynolds equation for the problem can be defined as:

$$Re = \frac{\rho \omega h^2}{\mu} \tag{7}$$

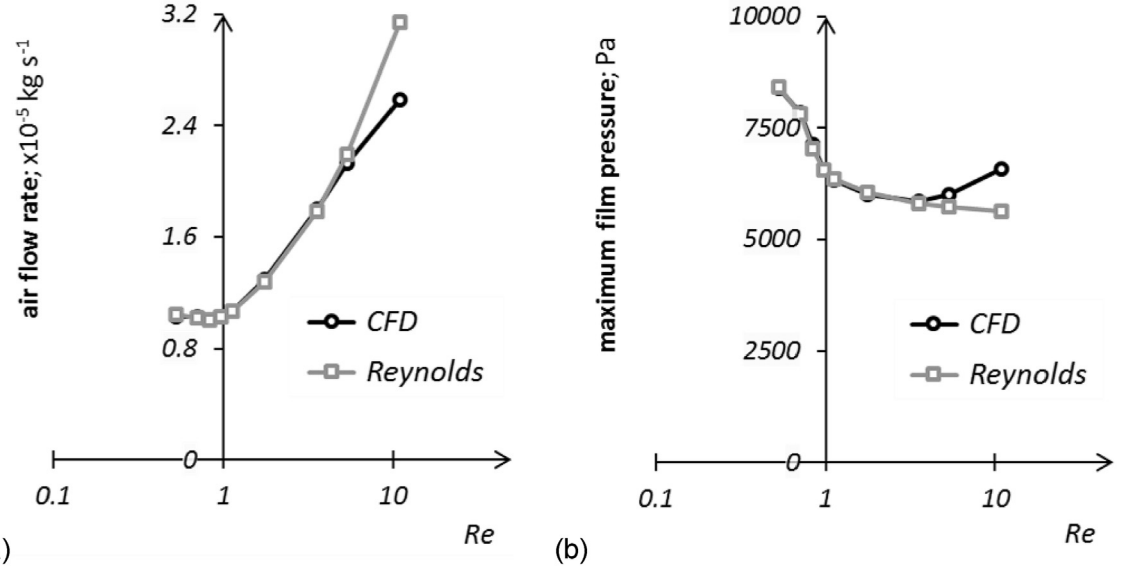

Fig. 7. Air flow, $x10^{-5}$ kg s^{-1}; (a) and maximum pressure Pa; (b) as a function of Reynolds number, comparison between CFD and Reynolds model results.

where h is the averaged levitation height in one period. Fig. 4 shows the levitation height calculated by both methods as a function of the oscillation frequency. It has been replotted as a function of Reynolds number in Fig. 6. It is clear from this graph that the deviation occurs when the Re becomes higher than 1, confirming that the deviation is due to inertia effects in the gas flow.

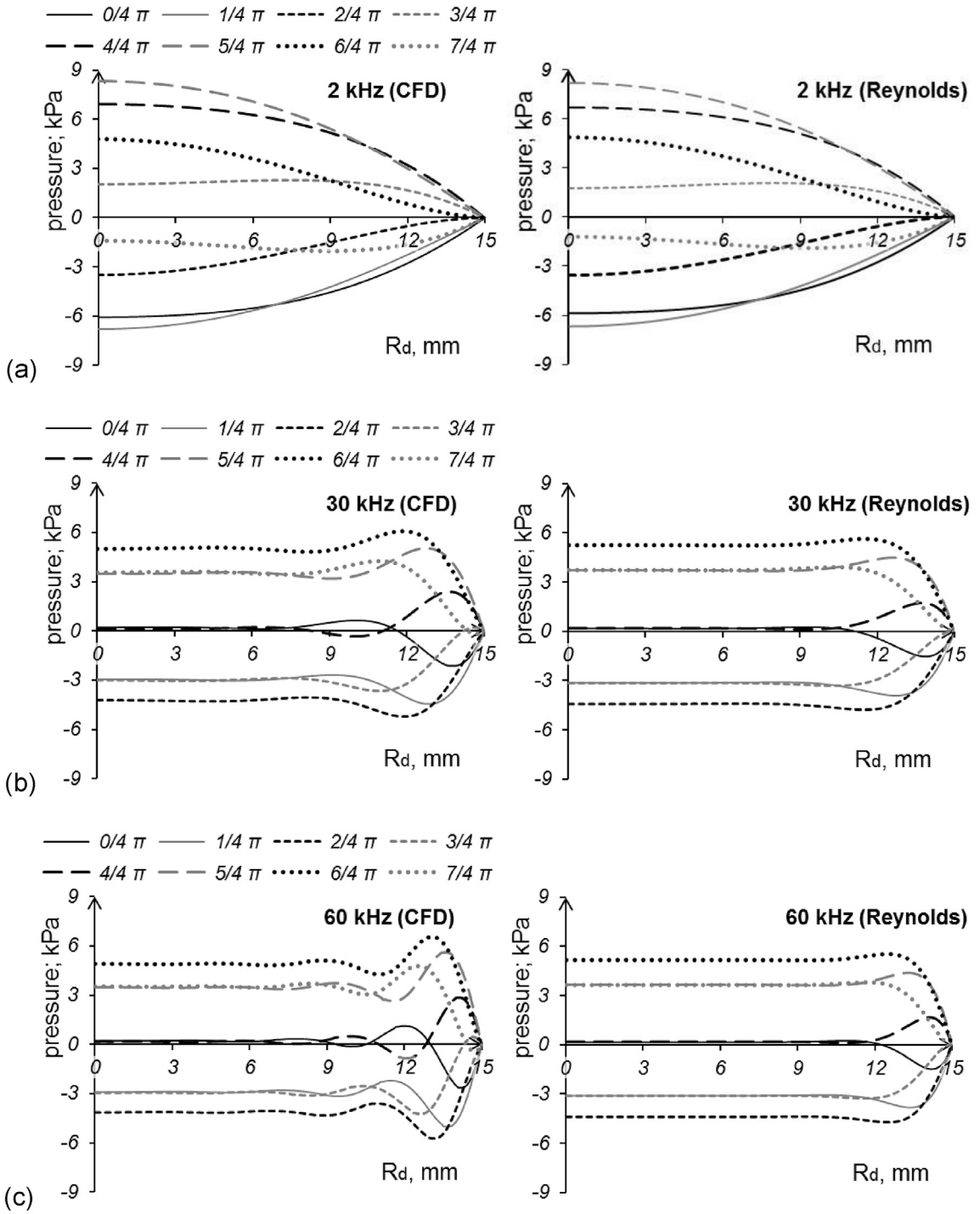

Fig. 8. Comparison of the calculated radial pressure profiles for selected time points of the oscillation period obtained from CFD and Reynolds models; (a) 2 kHz; (b) 30 kHz; (c) 60 kHz.

Doing the same analysis for the maximum pressure and air-flow presented in Fig. 5 does not give satisfactory results, as can be seen in Fig. 7. Indeed, the deviation starts at *Re* much higher than 1. Another physical phenomenon should explain this difference. This point is discussed in the following part of this section.

For a better understanding, pressure profiles in the air film along the radial direction are presented at different oscillation time steps obtained at different vibrating frequency values, f (see Fig. 8).

The difference between the pressure profiles from the NS and Reynolds methods is presented in Fig. 9.

At low f value (2 kHz), the results of the two methods are very close, the difference being less than 0.3 kPa. When the frequency is raised to 30 kHz, some differences between CFD and Reynolds can be observed. Some waves are visible on the pressure profiles obtained with the CFD solution. These waves are more pronounced at higher f values, the difference reaching 1.2 kPa. These waves explained the difference in maximum pressure and airflow between the CFD and Reynolds solution. These waves at high frequencies could be due to acoustic waves propagation which cannot be captured by the simplified Reynolds equation. Indeed, since the fluid inertia terms are neglected in the Reynolds equation, it is not possible to simulate acoustic waves which are the results of the fluid compressibility and fluid inertia interaction.

To analyze this assumption, the Helmholtz number of the flow, defined as the ratio of the time necessary for acoustic waves to travel across the contact divided by the oscillation period, is used. It is:

$$H = \frac{R_d f}{a} \tag{8}$$

where a is the speed of sound. When Fig. 5 is modified to be presented as a function of H, it appears that the deviation occurs when the Helmholtz number becomes higher than 1, confirming our assumption (see Fig. 10). When the oscillation period is lower than the time necessary for the pressure information to travel across the contact, a change in behavior is observed. This change cannot be captured by the Reynolds equation.

To analyze more deeply the effect of the acoustic waves propagation on the simulation results, air velocity profiles across the film thickness at $r = 14$ mm calculated with the use of Reynolds and CFD solutions were compared in Fig. 11.

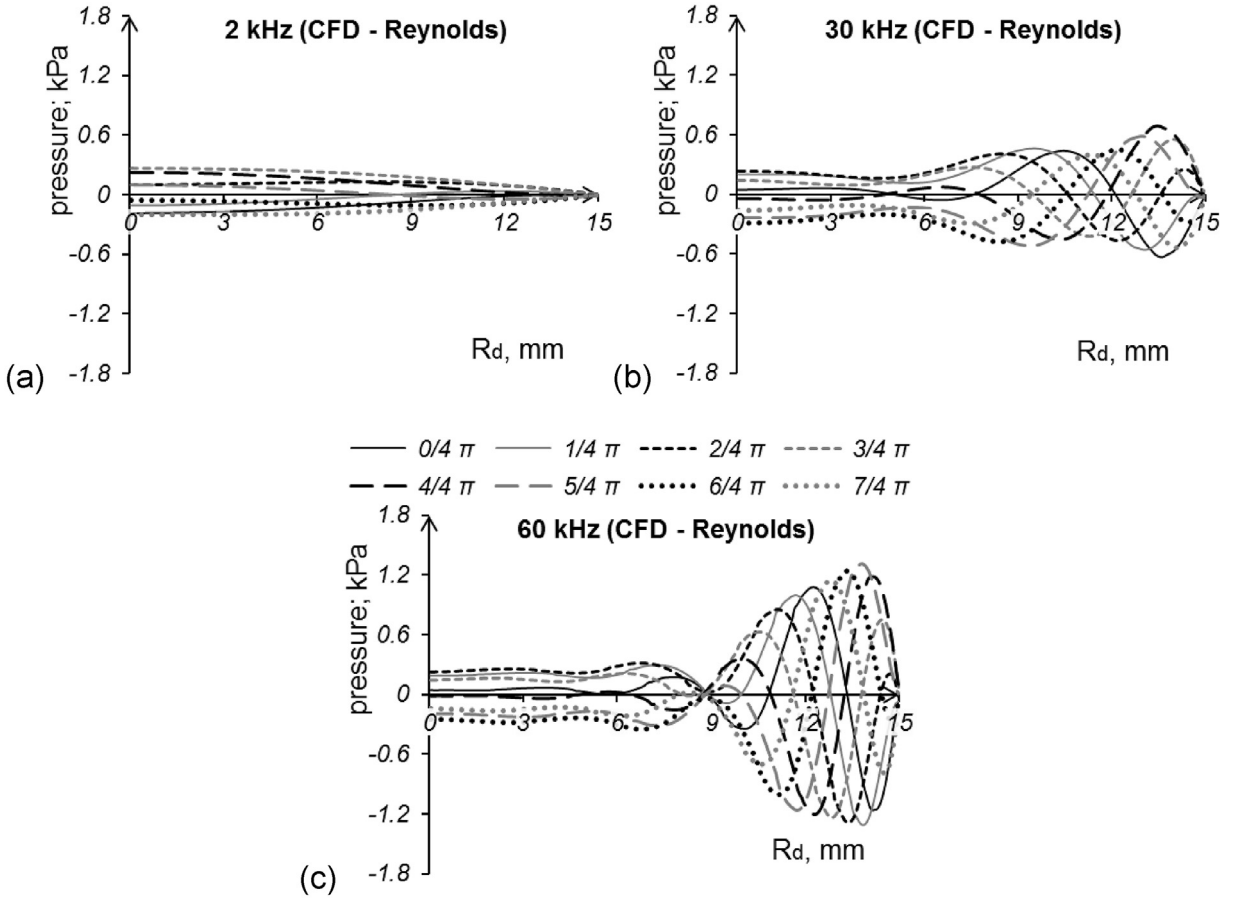

Fig. 9. Difference in pressure profiles obtained from the CFD and Reynolds models; (a) 2 kHz; (b) 30 kHz; (c) 60 kHz.

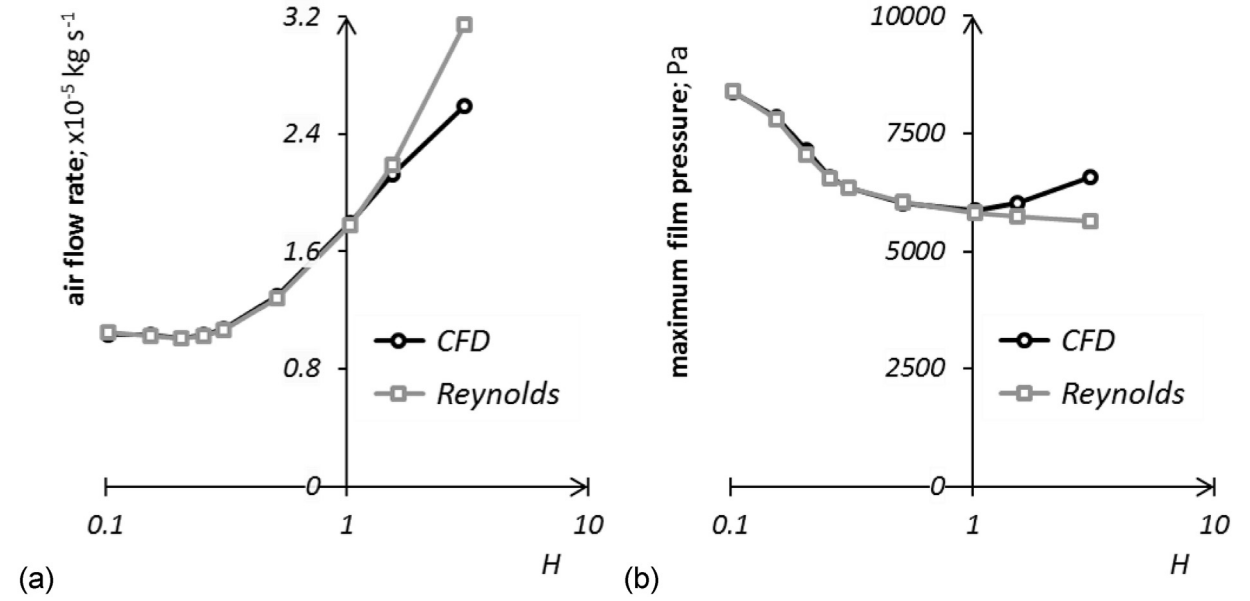

Fig. 10. Maximum air flow, x10^{-5} kg s^{-1}; (a) and maximum pressure, Pa, (b) as a function of Helmholtz number, comparison between CFD and Reynolds model results.

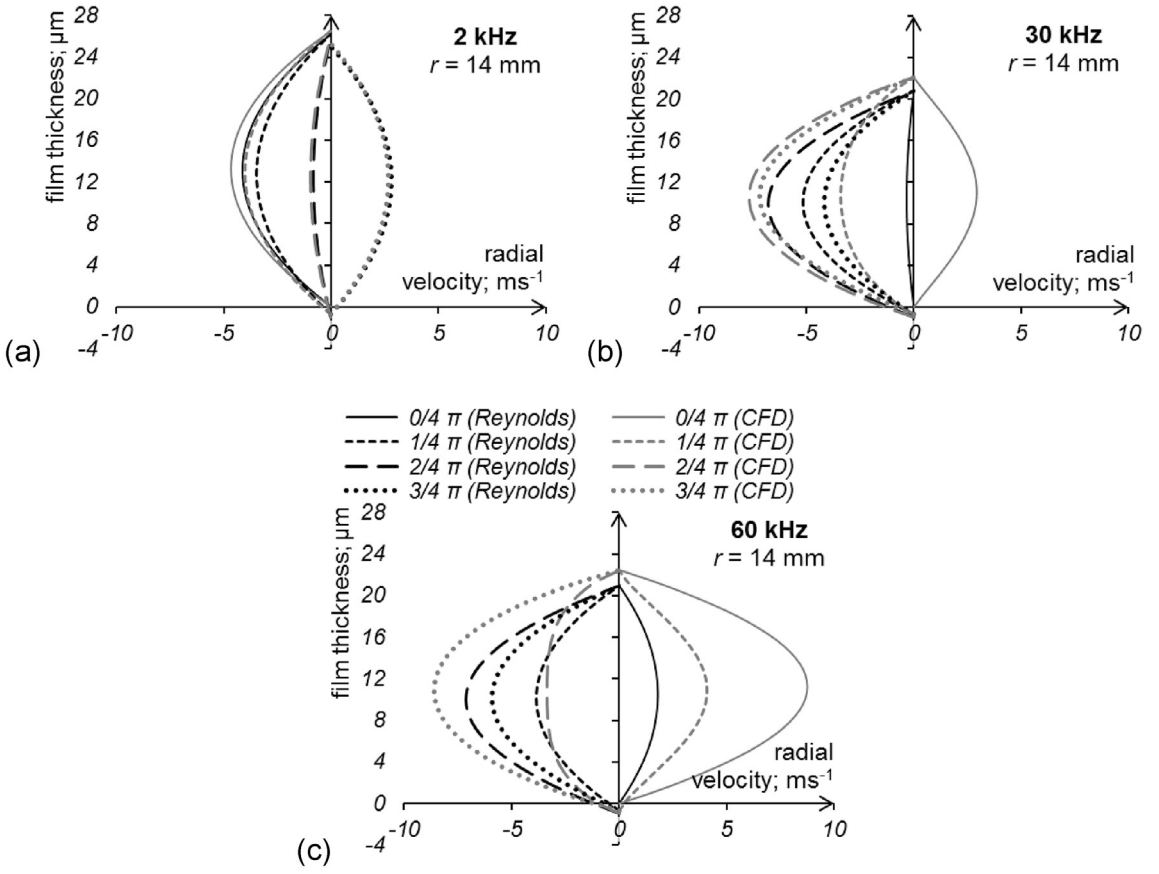

Fig. 11. Comparison of the calculated velocity profiles across air gap (at $r = 14$ mm) for selected time points of the oscillation period obtained from CFD and Reynolds models; (a) 2 kHz; (b) 30 kHz; (c) 60 kHz.

First of all, it can be seen that at H values much lower than 1, the velocity profiles obtained with both approaches are very close and with a parabolic shape (2 kHz case, Fig. 11a). When the frequency is increased to get H values higher than 1 (Fig. 11b and c), some significant differences can be observed. CFD solution showed that the velocity profiles are no more parabolic certainly because of the fluid acceleration which can be significant at high frequency. Secondly, the velocity profiles calculated with the Reynolds solution are, at some particular time period, inverted (show different direction of the local flow) when compared to the CFD solution. This is due to the pressure gradients that are not correctly calculated with the Reynolds equation. Indeed, the pressure waves can provide pressure gradient inversions not captured with the Reynolds equation (see Fig. 8). This last part clearly confirms, that when the Helmholtz number is higher than 1, air flow in the NFL system should be analyzed with the use of Navier-Stokes set of equations.

7. Summary and conclusion

The gas flow in an NFL system can be simulated by the Navier-Stokes approach, which is more general, and the Reynolds equation, which is a simplified approach. The latter has the advantage of a very low computation time.

These two methods were satisfactory compared to experiments performed on a levitated disk at low-frequency values (a few kHz). However, many near field levitation systems work at high frequency (several 10 kHz) for which the Reynolds equation is not necessarily valid. A comparison of the results obtained with the two methods was performed on a range of frequencies.

It was shown that, as expected, the Reynolds method deviates from the NS solution when the Reynolds number (Eq. (6)) is higher than 1. A second deviation was observed at higher oscillation frequency. It appears when the plate oscillation period is shorter than the time necessary for pressure information to radially travel through the gas film. It exactly corresponds to a Helmholtz number (Eq. (7)) of 1. Above this value, some acoustic pressure waves, which cannot be captured by the Reynolds equation, appear in the gas film.

It is thus necessary to check these two conditions before using the Reynolds equation to simulate the gas flow during near field acoustic levitation.

CRediT authorship contribution statement

Noël Brunetière: Conceptualization, Methodology, Software, Investigation, Validation, Writing - review & editing. **Michał Wodtke:** Conceptualization, Methodology, Investigation, Writing - original draft, Visualization.

Acknowledgments

This work was partially carried out as a part of research grant no. 2016/23/B/ST8/00210 entitled “Study on the use of Poisson's acoustic levitation effect for non-contact transportation of light objects” financed by the Polish National Science Centre.

CFD calculations were carried out at the Academic Computer Centre (TASK) in Gdańsk.

This work pertains to the French Government program “Investissements d'Avenir” (LABEX INTERACTIFS, reference ANR-11-LABX-0017-01).

References

[1] V. Vandaele, P. Lambert, A. Delchambre, Non-contact handling in microassembly: acoustical levitation, Precis. Eng. 29 (2005) 491–505, https://doi.org/10.1016/j.precisioneng.2005.03.003.
[2] T.A. Stolarski, Self-lifting contacts: from physical fundamentals to practical applications, Proc. Inst. Mech. Eng. Part C J Mech Eng Sci 220 (2006) 1211–1218, https://doi.org/10.1243/09544062JMES187.
[3] E.O.J. Salbu, Compressible squeeze films and squeeze bearings, J Basic Eng 86 (1964) 355–364, https://doi.org/10.1115/1.3653080.
[4] J.V. Beck, W.G. Holliday, C.L. Strodtman, Experiment and analysis of a flat disk squeeze-film bearing including effects of supported mass motion, J Lubr Technol 91 (1969) 138–148.
[5] Y. Hashimoto, Y. Koike, S. Ueha, Acoustic levitation of planar objects using a longitudinal vibration mode, J Acoust Soc Japan 16 (1995) 189–192, https://doi.org/10.1250/ast.16.189.
[6] S. Ueha, Y. Hashimoto, Y. Koike, Non-contact transportation using near-field acoustic levitation, Ultrasonics 38 (2000) 26–32, https://doi.org/10.1016/S0041-624X(99)00052-9.
[7] D. Ilssar, I. Bucher, On the slow dynamics of near-field acoustically levitated objects under High excitation frequencies, J. Sound Vib. 354 (2015) 154–166, https://doi.org/10.1016/j.jsv.2015.05.020.
[8] N. Brunetière, A. Blouin, G. Kastane, Conditions of lift-off and film thickness in squeeze film levitation, J. Tribol. 140 (2018), https://doi.org/10.1115/1.4038805, 031705-031706.
[9] Y. Hashimoto, Y. Koike, S. Ueha, Near-field acoustic levitation of planar specimens using flexural vibration, J. Acoust. Soc. Am. 100 (1996) 2057–2061, https://doi.org/10.1121/1.417915.
[10] A. Minikes, I. Bucher, Coupled dynamics of a squeeze-film levitated mass and a vibrating piezoelectric disc: numerical analysis and experimental study, J. Sound Vib. 263 (2003) 241–268, https://doi.org/10.1016/S0022-460X(02)01121-5.
[11] W. Li, Y. Liu, K. Feng, Modelling and experimental study on the influence of surface grooves on near-field acoustic levitation, Tribol. Int. 116 (2017) 138–146, https://doi.org/10.1016/j.triboint.2017.07.012.
[12] T.A. Stolarski, Y. Xue, S. Yoshimoto, Air journal bearing utilizing near-field acoustic levitation stationary shaft case, Proc. Inst. Mech. Eng. Part J J. Eng. Tribol. 225 (2011) 120–127, https://doi.org/10.1177/2041305X10394956.

[13] M.A. Atherton, C. Mares, T.A. Stolarski, Some fundamental aspects of self-levitating sliding contact bearings and their practical implementations, Proc. Inst. Mech. Eng. Part J J Eng Tribol 228 (2014) 916–927, https://doi.org/10.1177/1350650113517110.
[14] T.A. Stolarski, R. Gawarkiewicz, K. Tesch, Acoustic journal bearing - a search for adequate configuration, Tribol. Int. 92 (2015) 387–394, https://doi.org/10.1016/j.triboint.2015.07.019.
[15] T.A. Stolarski, R. Gawarkiewicz, K. Tesch, Acoustic journal bearing-Performance under various load and speed conditions, Tribol. Int. 102 (2016) 297–304, https://doi.org/10.1016/j.triboint.2016.05.048.
[16] S. Zhao, S. Mojrzisch, J. Wallaschek, An ultrasonic levitation journal bearing able to control spindle center position, Mech. Syst. Signal Process. 36 (2013) 168–181, https://doi.org/10.1016/j.ymssp.2012.05.006.
[17] T.A. Stolarski, M. Miyatake, Acoustic journal bearing with changeable geometry and built-in flexibility, J. Tribol. 140 (2018) 61707–61709, https://doi.org/10.1115/1.4040416.
[18] Y. Hashimoto, Y. Koike, S. Ueha, Transporting objects without contact using flexural traveling waves, J. Acoust. Soc. Am. 103 (1998) 3230–3233, https://doi.org/10.1121/1.423039.
[19] E. Matsuo, Y. Koike, K. Nakamura, S. Ueha, Y. Hashimoto, Holding characteristics of planar objects suspended by near-field acoustic levitation, Ultrasonics 38 (2000) 60–63, https://doi.org/10.1016/S0041-624X(99)00046-3.
[20] R. Gabai, D. Ilssar, R. Shaham, N. Cohen, I. Bucher, A rotational traveling wave based levitation device – modelling, design, and control, Sensors Actuators, A Phys. 255 (2017) 34–45, https://doi.org/10.1016/j.sna.2016.12.016.
[21] B. Wei, R. Shaham, I. Bucher, Theoretical investigation and prototype design for non-parallel squeeze film movement platform driven by standing waves, Tribol. Int. 119 (2018) 539–548, https://doi.org/10.1016/j.triboint.2017.10.034.
[22] B. Wei, R. Shaham, I. Bucher, J. Luo, Tangential motion mechanism and reverse hydrodynamic effects of acoustic platform with nonparallel squeeze film, Proc. Inst. Mech. Eng. Part J J Eng Tribol 233 (2019) 194–204, https://doi.org/10.1177/1350650118774426.
[23] H. Nomura, T. Kamakura, K. Matsuda, Theoretical and experimental examination of near-field acoustic levitation, J. Acoust. Soc. Am. 111 (2002) 1578–1583, https://doi.org/10.1121/1.1453452.
[24] O. Reynolds, On the theory of lubrication and its application to mr, Beauchamp Tower's Experiments. Proc R Soc London. 177 (1886) 157–234, https://doi.org/10.1098/rspl.1886.0021.
[25] I.B. Crandall, The air-damped vibrating system: theoretical calibration of the condenser transmitter, Phys Rev 11 (1918) 449–460, https://doi.org/10.1103/physrev.11.449.
[26] W.E. Langlois, Isothermal squeeze films, Q. Appl. Math. 20 (1962) 131–150, https://doi.org/10.1090/qam/99963.
[27] M. Andrews, I. Harris, G. Turner, A comparison of squeeze-film theory with measurements on a microstructure, Sensors Actuators A Phys 36 (1993) 79–87, https://doi.org/10.1016/0924-4247(93)80144-6.
[28] T.A. Stolarski, Numerical modeling and experimental verification of compressible squeeze film pressure, Tribol. Int. 43 (2010) 356–360, https://doi.org/10.1016/j.triboint.2009.06.015.
[29] J.E. Garratt, K.A. Cliffe, S. Hibberd, H. Power, A compressible flow model for the air-rotor-stator dynamics of a high-speed, squeeze-film thrust bearing, J. Fluid Mech. 655 (2010) 446–471, https://doi.org/10.1017/S0022112010000947.
[30] S.S. Mohite, V.R. Sonti, R. Pratap, A compact squeeze-film model including inertia, compressibility, and rarefaction effects for perforated 3-D MEMS structures, J Microelectromechanical Syst 17 (2008) 709–723, https://doi.org/10.1109/JMEMS.2008.921675.
[31] T.A. Stolarski, W. Chai, Inertia effect in squeeze film air contact, Tribol. Int. 41 (2008) 716–723, https://doi.org/10.1016/j.triboint.2007.12.008.
[32] J. Li, W. Cao, P. Liu, H. Ding, Influence of gas inertia and edge effect on squeeze film in near field acoustic levitation, Appl. Phys. Lett. 96 (2010), https://doi.org/10.1063/1.3455896, 243507-3.
[33] A. Minikes, I. Bucher, Comparing numerical and analytical solutions for squeeze-film levitation force, J. Fluid Struct. 22 (2006) 713–719, https://doi.org/10.1016/j.jfluidstructs.2006.02.004.
[34] ANSYS CFX -pre theory guide, Release 18 (2017) 2.
[35] M. Fillon, M. Wodtke, M. Wasilczuk, Effect of presence of lifting pocket on the THD performance of a large tilting-pad thrust bearing, Friction 3 (2015) 266–274, https://doi.org/10.1007/s40544-015-0092-4.